Effect of DEM Uncertainty on the Positional Accuracy of Airborne Imagery

Johan Beekhuizen, Gerard B. M. Heuvelink, Jan Biesemans, and Ils Reusen

***Abstract*—The geometric and atmospheric processing of airborne imagery is a complex task that involves many correction steps. Geometric correction is particularly challenging because slight movements of the aircraft and small changes in topography can have a great impact on the geographic positioning of the processed imagery. This paper focused on how uncertainty in topography, represented by a digital elevation model (DEM), propagates through the geometric correction process. We used a Monte Carlo analysis, in which, first, a geostatistical uncertainty model of the DEM was developed to simulate a large number of DEM realizations. Next, geometric correction was run for each of the simulated DEMs. The analysis of the corrected images and their variability provided valuable information about the positional accuracy of the corrected image. The method was applied to a hyperspectral image of a mountainous area in Calabria, Italy, by using the Shuttle Radar Topography Mission-DEM as the topographic information source. We found out that the uncertainty varies greatly over the whole terrain and is substantial at large off-nadir viewing angles in the across-track direction. Also, positional uncertainty is larger in rugged terrains. We conclude that Monte Carlo uncertainty propagation analysis is a valuable technique in deriving quality layers that inform end users about the positional accuracy of airborne imagery, and we recommend that it is integrated in the operational processing steps of the Processing and Archiving Facilities.**

***Index Terms*—Digital elevation model (DEM), error propagation, geometric correction, georeferencing, geostatistics, Monte Carlo simulation, orthorectification, uncertainty.**

I. Introduction

HIGH-RESOLUTION airborne imagery provides ample opportunities in analyzing the environment [1]. However, mounting a sensor on an airborne platform also brings great challenges in processing the retrieved data. The Processing and Archiving Facility (PAF) corrects the raw sensor data by consecutively applying correction algorithms, ranging from sensor calibration to geometric and atmospheric correction. An exemplary description of the PAF components can be found in [2] and [3]. This paper focuses on the geometric correction component.

Changes in the attitude and position of the aircraft and topography variation cause distortions in the geometry of the recorded image [4]. Geometric correction coregisters the pixel locations of the derived imagery with a real-world location. For airborne line scanners, geometric correction is preferably divided into two main steps [5]: the georeferencing and resampling steps. Splitting the geometric correction process allows that all subsequent atmospheric correction algorithms which need the pixel position, viewing, and illumination geometry perform their work on the raw scene geometry (and thus with noninterpolated pixels). Image resampling with associated pixel interpolation schemes (e.g., bilinear, cubic, and distance weighted) to a certain projection system and projection datum is done at the very end.

Geometrical correction of airborne imagery is difficult [1], and a physically exact representation of the scan geometry is required to reach (sub)pixel accuracy [6]. Retrieving the scan geometry requires knowledge of both the terrain and the position and look direction of the sensor [7]. The required information is obtained from the digital elevation model (DEM), GPS measurements, and attitude data from an inertial measurement unit (IMU), respectively. These data are the inputs of an advanced georeferencing technique that is called parametric orthorectification [6].

Brown *et al.* [7] modeled the geometric error in parametric orthorectification and found out that the DEM is a critical parameter because the DEM-derived parameters such as slope, elevation, and aspect are of great importance in geometric correction. They also showed that the error inflicted by the DEM errors depends on the viewing angle: the error will be smaller at nadir than at large off-nadir viewing angles. Insight in DEM error, uncertainty, and its propagation through the airborne image processing chain is therefore crucial.

The term "uncertainty propagation" is used here instead of "error propagation." Both terms are used in the literature (e.g., [8]–[11]) often to describe the same phenomenon, but it is important to make the distinction. Error is the difference between reality and a representation of reality. In practice, error is unknown because, if it was known, it would be eliminated. Uncertainty is the acknowledgement of error [12]. It is a property of people who realize that their representation of reality may deviate from reality itself. Uncertainty may be characterized with a probability distribution by listing all of the possible outcomes of reality and their associated probability (but note that only one of these can be the true reality, and it is the uncertainty about it that invokes the use of a probability

Manuscript received November 30, 2009; revised May 28, 2010 and September 6, 2010; accepted September 18, 2010. Date of publication December 10, 2010; date of current version April 22, 2011. This work was supported in part by the European Community's Seventh Framework Program (FP7/2007-2013) under Grant 227159 (European Facility for Airborne Research in Environmental and Geo-sciences).

J. Beekhuizen and G. B. M. Heuvelink are with the Land Dynamics Group, Wageningen University, 6708 PB Wageningen, The Netherlands (e-mail: gerard.heuvelink@wur.nl).

J. Biesemans and I. Reusen are with the Research Unit Remote Sensing and Earth Observation Processes, Flemish Institute for Technological Research (VITO), 2400 Mol, Belgium.

Color versions of one or more of the figures in this paper are available online at http://ieeexplore.ieee.org.

Digital Object Identifier 10.1109/TGRS.2010.2083672

distribution). Both error and uncertainty propagate in processing, but only uncertainty propagation can be traced because the error is unknown.

Much research has focused on determining the uncertainty and quality of a DEM (e.g., [13]–[17]) and its impact on the model outcomes (e.g., [18] and [19]). A suitable way in combining modeling DEM uncertainty and exploring its impact is by means of stochastic simulation [20], where many DEM realizations are simulated, representing the range of possible true elevations. In case ground control points (GCPs) are available, the simulation can be conditioned to these points. DEM realizations can subsequently be used as model inputs in a Monte Carlo uncertainty propagation analysis [21], [22].

In this paper, we use a similar approach, where we sample from a stochastic model representing DEM uncertainty, and subsequently perform a Monte Carlo analysis using the DEM samples. This has often been done before (e.g., [10] and [23]–[25]), but to our knowledge, no Monte Carlo analysis has explicitly focused on the impact of DEM uncertainty on the geometric correction of airborne imagery. Thus, the objective of this paper is to analyze how DEM uncertainty propagates through the geometric correction process and affects the positional accuracy of the derived imagery.

II. Methodology

A. Monte Carlo Method for Uncertainty Propagation Analysis

The objective of an uncertainty propagation analysis is to explore how the uncertainties in the model input data, model parameters, and model structure propagate to the model outputs [8]. Analytical approaches to error propagation are suitable in case of simple models that are (nearly) linear in their uncertain inputs, but these become cumbersome and involve approximations when the model is complex and highly nonlinear [8]. In such cases, a more convenient approach to uncertainty propagation analysis is to make use of Monte Carlo stochastic simulation, which can be applied to the geometric correction model as follows. First, N (typically $N \geq 100$) DEM realizations are simulated from a probabilistic uncertainty model. Next, the geometric correction model is run for each of the simulated inputs. This creates a sample of outputs whose statistical properties are derived and presented. In particular, the spread in the model outputs characterizes how the uncertainty about the model inputs has propagated to the model output. The Monte Carlo simulation approach for the DEM uncertainty propagation analysis is divided into the following three steps and is described in Sections II-B–D.

1) Define a probabilistic DEM uncertainty model (Section II-B).
2) Estimate the required number of Monte Carlo runs N, and generate N DEM realizations by repeated sampling from the uncertainty model (Section II-C).
3) Run the geometric correction for the N simulated DEMs, and analyze the results (Section II-D).

B. DEM Uncertainty Model

The DEM uncertainty model characterizes the true elevation at any location within the study area by means of a (marginal) probability distribution. However, the spatial correlation must also be specified because the DEM uncertainties are typically spatially correlated, which can have a great impact on the uncertainty propagation analysis [8]. Therefore, geostatistical techniques are frequently used. Geostatistical simulation methods often invoke the (second-order) stationarity assumption, which states that the mean and variance of the uncertainty distribution are constant in space and that the spatial covariance only depends on the distance between locations and not on their exact locations. The spatial covariance is characterized by a semivariogram [26]. Although assumptions are needed to build an uncertainty model from limited information (i.e., the observed errors at control points; see later), the assumption of constant variance seems unrealistic for DEM applications. Instead, it is more realistic to assume that the variance depends on the ruggedness (or roughness) of the terrain (e.g., [14] and [24]). Therefore, we defined a model in which the standard deviation of the uncertainty about the true elevation Z is proportional to the terrain ruggedness

$$Z(x) = \text{dem}(x) + R(x). \tag{1}$$

Here, $\text{dem}(x)$ is the DEM-derived elevation at location x, which is known and deterministic. $R(x)$ is a stochastic residual that represents the DEM error, which satisfies

$$R(x) = r(x) \cdot R_s(x) \tag{2}$$

where $r(x)$ is the ruggedness at x, computed from the DEM, and where $R_s(x)$ is the standardized residual, which is assumed to be second-order stationary. In addition, we also assume that R_s is normally distributed. Thus, R_s is fully characterized by its mean, variance, and semivariogram. Note that the variance of R_s is identical to the sill of its semivariogram.

Ruggedness Calculation: The ruggedness $r(x)$ at a location x may be defined as the standard deviation of all DEM heights in a kernel or window of $p \times p$ pixels centered around x. The optimum value for the kernel width p can be found by calculating the "error-ruggedness" correlations for different kernel widths and by selecting the width with the greatest correlation coefficient.

Sampling Control Points and Semivariogram Estimation: The elevations at the control points are required to estimate the mean and semivariogram of R_s. At the control points, the true elevation is measured with a negligible measurement error, and the DEM error is computed by subtracting the DEM elevation from the true elevation. The number and spatial configuration of the control points must be chosen such that a reliable estimation of the semivariogram is obtained. The semivariogram $\gamma(h)$ [27] describes the spatial dependence between the standardized residuals as follows:

$$\gamma(h) = \frac{1}{2} E\left[\left(R_s(x) - R_s(x+h)\right)^2\right] \tag{3}$$

where E is the mathematical expectation and h is the lag distance. Since we only know the residuals at the control points, the semivariogram is based on all of the paired comparisons of the residuals at the control points. This yields the experimental

semivariogram. Next a semivariogram model is fitted through the experimental semivariogram, which describes the spatial dependence semivariogram for all distances [26].

The optimal configuration of the sampling locations depends on the semivariogram and the range of spatial correlation [28]. However, since we do not know the semivariogram *a priori*, an alternative criterion is to ensure that there are enough point pairs for all lag distances h. It is not easy to decide how many control points are needed, since this depends on various factors such as the sampling configuration, the semivariogram estimation method, the shape of the study area, and the required level of reliability. As a rule of thumb, at least 100 points are recommended [29].

By considering the aforementioned discussion, a sampling design procedure that is based on a balanced nested design [29] is proposed, which can be implemented as follows: first, the area is divided into regions of (approximately) equal sizes. Next, in each region, an equal number of control points are sampled by starting in the center of the region and by selecting one or more points at a given distance and random angle from the region center. The distance is chosen such that the point is located in the region. The point in the opposite direction from the center is also added. These points serve as centers for the next sampling round, where the same procedure is repeated, but now with a much smaller distance. The nested sampling procedure guarantees that a sufficient information is gathered about the short-distance spatial variability while maintaining a fairly uniform distribution over the study area.

C. Stochastic Simulation of the DEM Realizations

After defining the semivariogram, control points, and ruggedness, the realizations of R_s are created using a conditional sequential Gaussian simulation [26]. Briefly, this works as follows. Each location (grid cell) of the spatial domain is visited in a random sequence. At each location, the conditional probability distribution of R_s is computed. For the first location, this is obtained with simple kriging, using the observations of R_s as conditioning data. Next, a value from the conditional probability distribution is drawn using a pseudorandom number generator. The simulated value is assigned to the location and is added to the data set. At the second location, the procedure is repeated, again using simple kriging to condition it to the data set, which now also includes the simulated value at the first location. The procedure is repeated until all of the grid cells have been visited. Note that the simulated values at the previous grid cells must all be included in the data set when simulating at the next cell to ensure that the simulated DEM is a realization from a random function with the specified spatial correlation structure.

The simulated realities R_s are transformed to the simulated realities of R by multiplying it with the ruggedness r. Next, the stochastic residuals R are added to the DEM. This creates DEM realizations which are used as inputs to the Monte Carlo uncertainty propagation analysis. Because the geometric correction is a time- and resource-consuming process, it is important to consider the number of required realizations N. In general, N must be large enough to guarantee that the outcome of the Monte Carlo analysis is sufficiently accurate.

The accuracy of the Monte Carlo method can be described by the coefficient of variation of the variance of the model outputs, computed as follows [8]:

$$\mathrm{cv}(S^2) = \sqrt{\frac{\gamma_2}{N} + \frac{2}{N-1}} \tag{4}$$

where S^2 is the variance of the model output U (i.e., the geographic coordinate of a pixel after geometric correction) and γ_2 is the coefficient of kurtosis. The kurtosis has to be calculated from the output, but if we assume a normal distribution, the kurtosis is zero. This enables us to compute the coefficient of variation before the actual Monte Carlo analysis, providing an indication of the number of required model runs. For instance, $N = 100$ yields $\mathrm{cv} = 0.14$, and $N = 1000$ yields $\mathrm{cv} = 0.04$.

When the objective is to estimate the variance of the model output with a known accuracy, N must be calculated based on the variance of the associated estimation error [8], [30]

$$\mathrm{Var}(S^2 - \sigma^2) \cong \frac{\mu_4 - \sigma^4}{N} \tag{5}$$

where σ^2 is the output variance, S^2 is its estimate, and μ_4 is the fourth central moment of the output. Under the assumption of normality, the fourth central moment is equal to $3\sigma^4$. Unlike the cv, the required Monte Carlo sample size cannot be computed beforehand because the output variance σ^2 is unknown. Equations (4) and (5) also show that the coefficient of variation and the standard deviation are inversely proportional to the square root of the sample size N. Thus, to halve the standard deviation or cv, one must quadruple the number of Monte Carlo runs.

Next to these analytical methods, an empirical approach may also be used to analyze whether the number of Monte Carlo runs used was sufficient and produced stable results. This can be done by repeating the Monte Carlo uncertainty propagation analysis and by plotting the results from the first against those of the second analysis. In the limit, when there are an infinite number of Monte Carlo runs, all points will lie on the 1:1 line. For a finite number of runs, there will be deviations from the line, and the magnitude of the deviation may be visually inspected to verify whether the Monte Carlo results were sufficiently stable.

D. Running the Geometric Correction Model for Each DEM Realization and Analysis of Results

Once all preparations are done and once N realizations of the DEM have been generated, the geometric correction algorithm is run for all realizations, and the results are analyzed. This requires that the geometric correction algorithm is sufficiently automated, and it can be repeatedly run in batch mode while storing results of all individual runs. It is recommended to first check the procedure by performing the analysis for a small subset.

The Monte Carlo analysis results in N geocorrected images, from which the positional accuracy must be derived. The analysis consists of calculating various statistical measures (notably, the standard deviation of the geographic positions). The analysis can be based on the comparison of the image geometry map (IGM) among all N Monte Carlo runs. The IGM

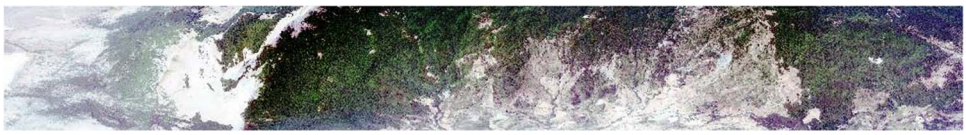

Fig. 1. True color composite of the AHS hyperspectral image of Calabria (before geometric correction).

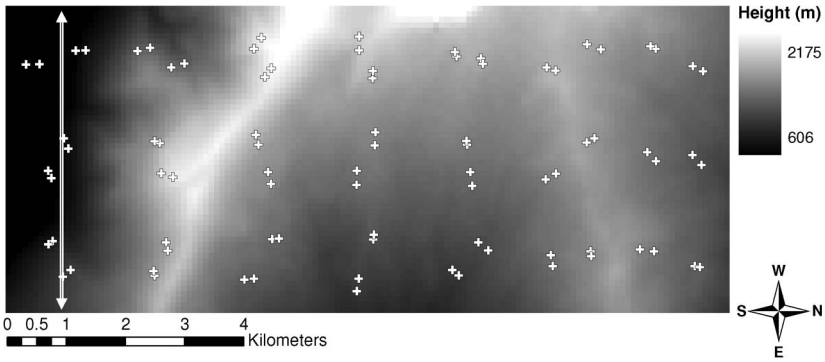

Fig. 2. SRTM-DEM. The white crosses represent the locations of the control points (Section IV-A), and the white line represents the location of the transect visualized in Fig. 7.

consists of two layers that contain the georeferenced x and y locations for each pixel of the geocorrected image.

The most basic statistic that can be derived from the set of IGMs is the mean value of the x and y coordinates for each pixel. The mean values do not provide any information about the uncertainty, but they can be used as a reference in calculating the deviation of one IGM from the average or (in case no other reference is available) as the single most likely output of all IGMs. In terms of uncertainty propagation, however, the more relevant statistics are the standard deviations of the x and y coordinates.

The end user may also be interested in the probability that the deviation of the projected coordinate with a reference coordinate (e.g., the mean) is greater or smaller than the size of one pixel, i.e., one is interested to know if a subpixel accuracy is achieved. Here, we assume that the subpixel accuracy is reached when both Δx (the deviation of x from the mean x coordinate) and Δy (the deviation of y from the mean y coordinate) are within the size of one pixel.

The subpixel probability can be computed by counting the number of times that both Δx and Δy are smaller than the pixel size and by dividing this number by the number of Monte Carlo runs N. The probability of failing to reach the subpixel accuracy (the "exceedance" probability) is one minus the probability of reaching the subpixel accuracy.

III. Study Area, Data, and Software

In order to study the impact of DEM uncertainty on the positional accuracy of airborne imagery, we performed a case study using a hyperspectral image of Calabria, Italy. The image covers an area of about 4 by 12 km, centered around a latitude of $16°24'$ and a longitude of $39°94'$. The area is rugged and mountainous, with altitudes ranging from 650 to 2260 m, and the dominant land cover types are forest and bare rock. The image (Fig. 1) was acquired by the Airborne Hyperspectral Scanner (AHS). The AHS is an 80-band airborne hyperspectral line scanner radiometer with a field of view (FOV) of 90° and an instantaneous FOV of 2.5 mrad [31]. The aircraft that was used to obtain the image flew at a mean altitude of 2680 m from north to south. The image was part of a larger data set that was acquired for an archaeological survey. As part of this survey, a LIDAR (Leica ALS50 LIDAR, 1 point per m^2) mission was performed to build a high-accuracy digital surface model (DSM).

The DEM that was used as the uncertain source in the geometric correction process was provided by the Shuttle Radar Topography Mission (SRTM). The SRTM recorded interferometric synthetic aperture radar data in the C- and X-bands and processed these data to C- and X-band DEMs [32]. The DEMs are freely available at a resolution of 1″ for the United States and 3″ (∼90 m) for other parts of the world [32]. We downloaded a gap-filled preprocessed C-band DEM [33] covering the whole study area (Fig. 2). The objective of the SRTM was to meet a ±6-m relative vertical accuracy for 90% of the data of the C-band 1″ DEM [34], [35].

As is common in airborne image processing, we assumed the availability of ground reference data in the study area. Due to a lack of field-measured GCPs, we simulated the collection of GCPs by sampling from the high-resolution LIDAR-DSM. A correctly processed LIDAR-DSM has an error of, at most, a few decimeters [36] (one order of magnitude smaller than the SRTM-DEM), and it was therefore assumed to represent the true elevation.

The geometric correction was performed with the in-house developed PAF of the Flemish Institute for Technological Research (VITO) [2]. For airborne sensors, the VITO-PAF uses the "direct georeferencing" parametric orthorectification procedure [37] in determining the position and attitude of the sensor plane. Direct georeferencing is the direct measurement of the position (by means of a GPS) and orientation parameters (by means of an IMU). Applying the orientation matrix on the GPS/IMU time-series combined with a ray-tracing algorithm (e.g., [38]) to determine the intersection position of the ray (from pixel to surface) with the DEM delivers the pixel position (X, Y, and Z). The georeferencing process is thus fully

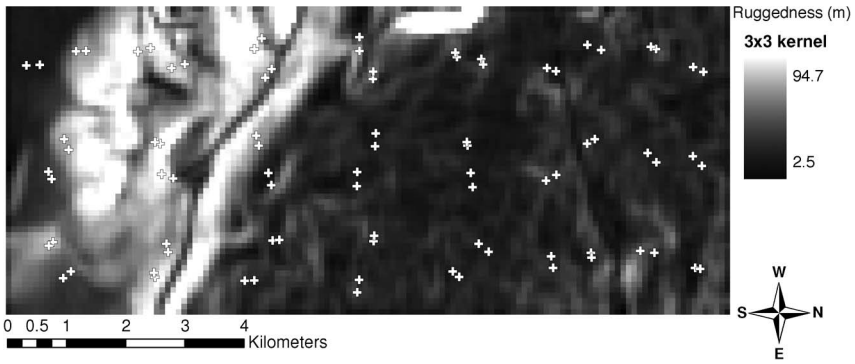

Fig. 3. Ruggedness map that is based on the elevation standard deviation of a 3 × 3 kernel.

analytical. The scripting of the Monte Carlo analysis was done in the statistical programming language R using the functionality of the geostatistical library gstat [39], [40].

IV. Results

A. DEM Uncertainty Model

Ruggedness Calculation: The ruggedness map was created by computing, for each pixel, the standard deviation of the SRTM-DEM heights in a kernel of $p \times p$ pixels. For large kernel sizes, the ruggedness map is smooth, and the importance of short range variation is small, whereas small kernel sizes accentuate short distance height variations. Fig. 3 shows a 3 × 3 kernel ruggedness map. As the SRTM-DEM has a pixel size of 90 m, this figure shows the ruggedness of the terrain in an area of 270 by 270 m.

Sampling Control Points: We created a sampling design for a total of 84 control points using the approach explained in Section II-B. In order to evenly distribute the sample over the whole area and to have enough close range points for the semivariogram estimation, we divided the 4 by 12 km large area in 3 × 7 rectangular regions, with four control points in each region. In each region, the first point was selected at random distance (uniformly sampled between 200 and 375 m) and angle from the region center. The location of the second point was defined by mirroring the first point around the region center. The two remaining control points per region were positioned at a random distance (uniformly sampled between 60 and 200 m) from the first two control points. The distances were chosen such that sufficient point pairs in all distance lags are available in computing the experimental semivariogram. The control points are plotted on the SRTM-DEM shown in Fig. 2. The DEM errors at the control points have a root mean square error of 15.6 and have exceeded the SRTM relative vertical accuracy objective: 49% (instead of the intended 90%) of the errors are smaller than 6 m. This may be explained by the combined effect of a mountainous study area and the use of the 3″, instead of the 1″, SRTM-DEM.

Correlation Ruggedness—DEM Error: The optimum kernel width value was found by exploring the correlations between the absolute DEM error and the ruggedness values at the control points, using different kernel sizes to compute varying ruggedness maps. As shown in Table I, a 3 × 3 kernel ruggedness map (kernel width of 270 m) resulted in the highest correlation with DEM error. We therefore used this kernel width for the ruggedness calculation. Fig. 4 shows the corresponding scatter plot of the ruggedness against the absolute DEM error.

TABLE I
Correlation Coefficients Between the Absolute DEM Error and the Ruggedness at the Control Points

Ruggedness Kernel width (m)	Correlation coefficient
270	0.552
450	0.528
630	0.522
810	0.509
990	0.493

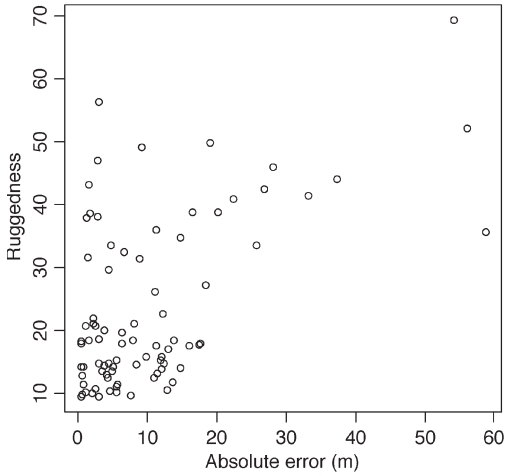

Fig. 4. Correlation between the 3 × 3 kernel ruggedness and the absolute DEM error.

Semivariogram Estimation: After sampling the control points and determining the optimum kernel width, the experimental semivariogram was computed, and the semivariogram model was determined (Fig. 5). We fitted a Matern model with a smoothness parameter of 0.6 [41], a zero nugget, a sill of 0.3, and a range of 270 m.

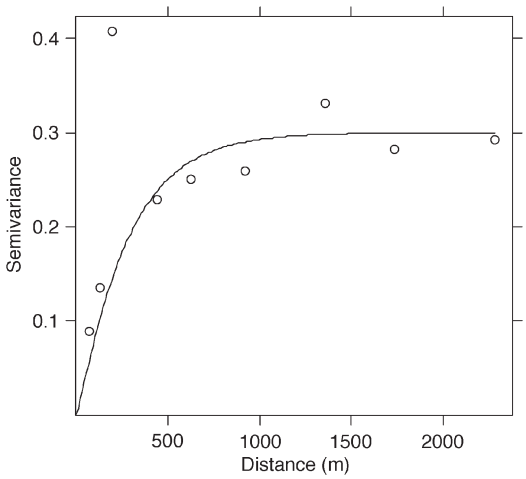

Fig. 5. Semivariogram of the standardized residuals at the control points. The circles represent the experimental semivariogram, and the black line indicates the fitted semivariogram model.

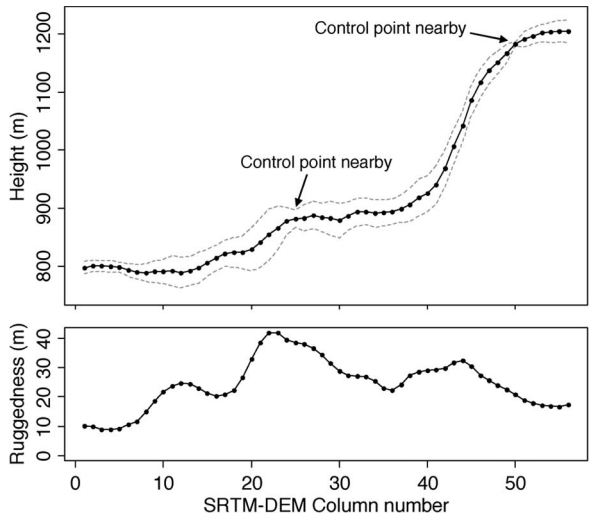

Fig. 6. Simulated DEMs and ruggedness along a transect (see Fig. 2 for the location). The top panel shows the mean height over all simulations (solid line) and the 95% confidence interval (the area in between dashed gray lines). The bottom panel shows the ruggedness.

B. Stochastic Simulation of the DEM Realizations

By considering the computation time, storage requirement, and Monte Carlo sampling error, we decided to use $N = 100$ Monte Carlo simulations. Under the assumption of a normal distribution, this yields a coefficient of variation for the estimated output variance of 0.14, which is not small, but it was considered acceptable. It means that the true output variance will lie within 28% of the estimated value in 95 out of 100 cases.

Fig. 6 shows a transect of the DEM realizations and ruggedness, located in the southern part of the study area (see the white line in Fig. 2). As imposed by the uncertainty model, there is a clear relationship between the standard deviation of the height and the ruggedness. In rugged areas, the standard deviation of the height is larger, indicating a larger uncertainty in the DEM heights, and in relatively smooth areas, the DEM uncertainty is smaller. There are two control points that are near the transect, resulting in less uncertainty and, thus, a narrower confidence interval.

Fig. 7 shows the standard deviation map of the DEM simulations. Again, there is a clear relationship between the standard deviation of the height and the ruggedness (compared with Fig. 3). At the location of the control points (indicated by the white crosses), the standard deviation of the height is smaller.

C. Analysis of the Monte Carlo Results

Fig. 8 shows one complete geocorrected image and cutouts of three different corrected images. Each of the cutouts refers to exactly the same area and is enlarged in order to visualize the uncertainty propagation of the geocorrected output. The images show the rugged terrain: the dark areas are the trees, and the light areas are the bare rock. The white cross shows the location of the control point. Around the control point, the spatial distortion is small, but farther away from it, the distortions are quite severe. This is particularly visible in the patch of forest in the upper-right corner of the images.

Fig. 9 shows the mean values of the IGM over all simulations for both the x and y coordinates. The figure shows the information content of the IGM. It stores the georeferenced world location for each of the 750×5000 pixels of the original raw image. Fig. 10 shows the standard deviation of the IGM over all simulations of the x and y coordinates. The standard deviation is relatively large (up to 16 m) for subareas with larger viewing angles and in more rugged terrain, and it is relatively small (below 4 m) in areas with small viewing angles and in areas that are close to the control points. Fig. 11 shows the probability of exceeding the subpixel accuracy for an output pixel size of 2.9 m. The output pixel size is the cell size of the regular grid where the georeferenced output is transformed in the resampling algorithm, and it is automatically determined in the geometric correction procedure. As expected, the exceedance probabilities are large in areas where the uncertainty about the geometric correction is large, and they are small in areas with small viewing angles and in areas that are near the control points. On average, the probability of exceeding the subpixel accuracy is 0.382.

D. Evaluation of the Monte Carlo Sample Size

In order to empirically determine whether 100 Monte Carlo runs are sufficient for reliable results, a second set of 100 Monte Carlo runs was done. Fig. 12 shows the scatter plot of the exceedance probabilities of set 1 against those of set 2. For visualization purposes, a random subset of 50 000 points out of the total of 3 750 000 points is shown. The graph shows a strong relationship between the two sets, which is confirmed by the R^2 of the exhaustive data sets of 0.983. Note the "gridded" pattern in the scatter plot, which is caused by the fact that all estimated probabilities are multiples of 0.01.

V. Discussion and Further Research

The IGM simulations obtained with the Monte Carlo method provide a valuable source of information about DEM

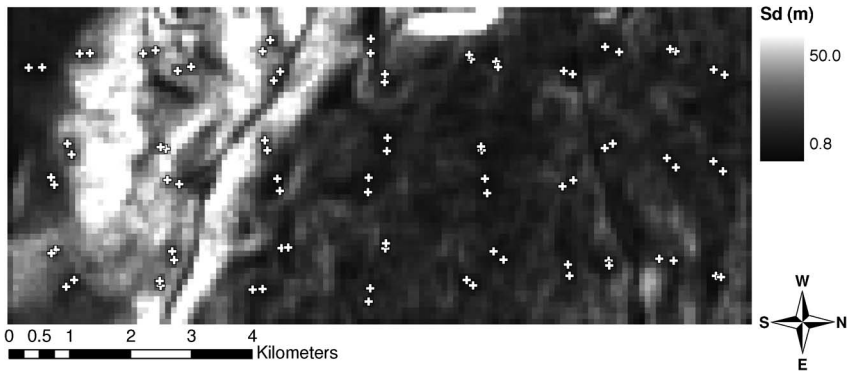

Fig. 7. Standard deviation of the DEM simulations. The control points are indicated by the white crosses.

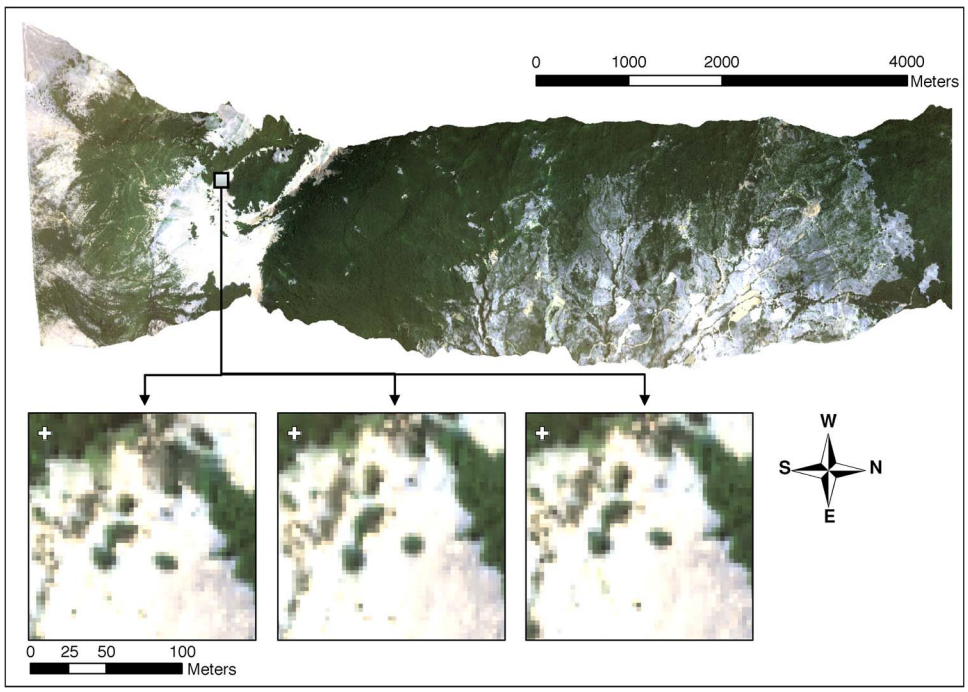

Fig. 8. One complete geometrically corrected image and three cutouts of different Monte Carlo simulations. The white cross shows the location of the control point.

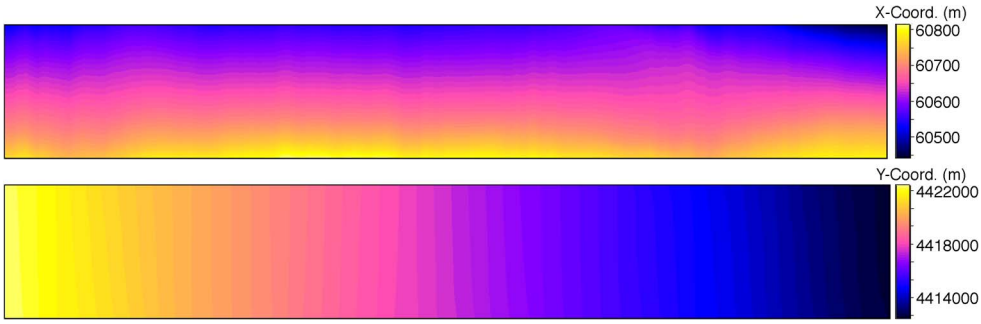

Fig. 9. IGM of the mean projected (top panel) x and (bottom panel) y coordinates in UTM projection.

uncertainty propagation in the geometric correction of airborne imagery. The standard deviation of the IGM over all simulations (of the x and y coordinates) can be used as a measure of the per-pixel positional uncertainty. However, the standard deviation is a scene-specific quality indicator of the positional accuracy since the output pixel size differs per output image. Thus, a standard deviation of 5 m might be large for one image but relatively small for another. Therefore, an exceedance probability map was also computed, showing the probability of failing to reach the subpixel accuracy.

The exceedance probability map showed that, in large areas, especially in rugged terrain, the subpixel accuracies are not

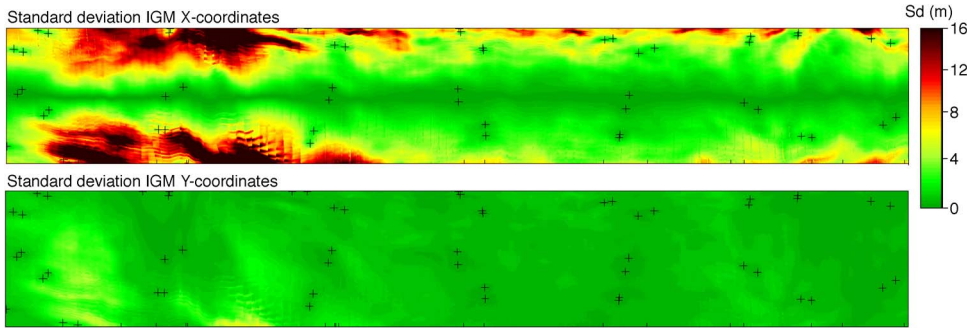

Fig. 10. Standard deviation (in meters) of the IGM (top) x and (bottom) y coordinates. The black crosses are the locations of the control points.

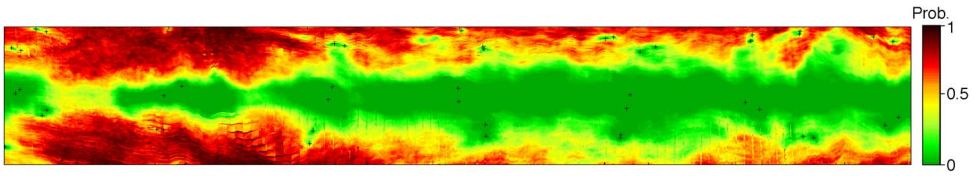

Fig. 11. Probability of failing the subpixel accuracy target (when either the x or y coordinate or both deviate more than one pixel width from the mean location). The pixel size is 2.9 m.

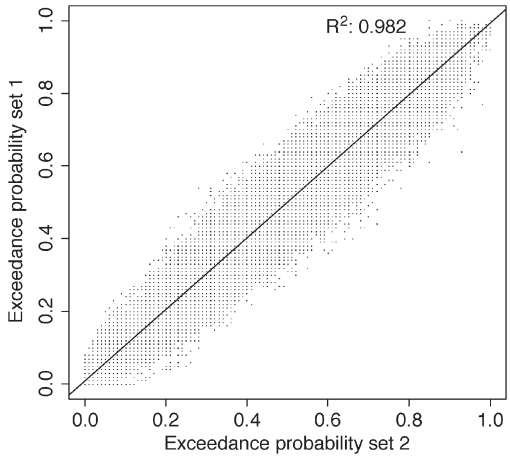

Fig. 12. Scatter plot of the exceedance probabilities of two independent Monte Carlo analyses.

reached. There is much less uncertainty in areas that are near the control points, but the uncertainty rapidly increases with distance. This can be explained by the relatively short range of 270 m (3 pixels) of the semivariogram model, which implies that, at a distance of 270 m, the uncertainty is no longer mitigated by the control points. Deviations occur in both the x and y directions, which can be explained by the ray-tracing algorithm [38] used in the VITO geometric correction procedure. Since each simulation uses another DEM, the 3-D positioning of the intersection of the pixel-dependent viewing ray with the DEM is changed, thus causing uncertainty in both the x and y directions. There is a larger uncertainty in the x coordinates than in the y coordinates, which is a result of the flight direction of the aircraft. Because the aircraft flew from north to south, the across-track direction is east–west, and the along-track direction is north–south. This leads to larger difficulties in estimating the x coordinates, especially at low flying altitudes and in mountainous areas, as was the case in this paper. These results confirm the findings of [7]: the largest deviations occur at large off-nadir viewing angles.

There is a distinct striping pattern in the standard deviation and exceedance probability maps, showing large differences between pixels at close range (see Figs. 10 and 11). This "staircase effect" is the result of the downscaling of the DEM realizations to the spatial resolution used in the geometric correction procedure. The DEM realizations with a pixel size of 90 by 90 m are too coarse for the output pixel size of 2.9 by 2.9 m.

Obviously, in reality, the SRTM-DEM would not be used in case a LIDAR-DSM is available. However, in flight campaigns in large parts of the world, the best DEM available is the SRTM-DEM. Even though there are advanced ways to correct SRTM-DEM errors that result from the radar-based retrieval method, such as shadowing, foreshortening, lay-over, noise removal, and vegetation cover correction (e.g., [34], [42]), these corrections are unlikely to be performed in a flight campaign and often depend on auxiliary data which might not be available. This paper aims to explore the effect of DEM uncertainty on the positional accuracy of geometrically corrected images in a realistic setting and not to obtain the highest quality SRTM-DEM.

The DEM uncertainty model strongly relies on both the semivariogram and the ruggedness of the terrain, and a critical assessment of both is appropriate. The semivariogram is based on a limited number of 84 control points, and it is therefore important that a suitable sampling design is chosen in order to obtain a reliable semivariogram model. The nested sampling approach seems effective, but for further research, other designs might be tried (e.g., [28] and [29]). Next, the DEM simulation depends on the correlation between the height errors and terrain ruggedness. We found a significant correlation of 0.552, indicating that including ruggedness yields a more realistic characterization of DEM uncertainty. Further research could extend the uncertainty model by including more terrain parameters, such as minimum extremity and slope [15], [24].

One of the main drawbacks of the Monte Carlo method is its computation time, since large data sets have to be processed N times. The total computation time for a complete DEM uncertainty propagation analysis ($N = 100$) is about 26 h on a Windows XP computer with Intel Core 2 Duo CPU and 3 GB of RAM. However, there are many ways to reduce the computation time. The Monte Carlo method is very suited for parallel computing and for the grid computing technology [43], which is a standard practice in many PAFs. In this way, the computation times can be dramatically reduced, provided that the equipment is available in large enough numbers. Next, in this case study, 100 Monte Carlo runs turned out to be sufficient in obtaining reliable results, shown both empirically and analytically. Depending on the desired accuracy, N may therefore be decreased. Also, it may be possible to further decrease N by increasing the efficiency of the sampling, e.g., by drawing Latin hypercube samples [44] from the conditional distribution of the uncertain input.

DEM uncertainty is also an important source of error for the atmospheric correction [45], where it is used in modeling the bidirectional reflectance distribution function. A similar Monte Carlo approach, as implemented in this paper, could explore the effect of DEM uncertainty on the estimation of the at-surface reflectance [46].

It is important to emphasize that the results of this paper do not show the total uncertainty in the geometric correction process, as the DEM is not the only source of uncertainty. First, the geometric correction model itself represents a source of uncertainty. Second, there are other uncertain model inputs such as the camera interior orientation parameters (FOV, focal length, and position of the principal point) and the camera exterior orientation parameters [the GPS/IMU time series and the boresight angles (i.e., the offset between the sensor and the IMU coordinate system)]. Further research could extend the Monte Carlo analysis with the other uncertain inputs to determine the combined effect of these parameters on the processed images or could use different geometric correction models to see how DEM uncertainty depends on the model used.

VI. Conclusion

In this paper, we have presented a (geo)statistical methodology that is used to analyze how DEM uncertainty affects the positional accuracy of airborne imagery on a pixel basis and have illustrated the methodology with a real-world case study. Monte Carlo uncertainty propagation analysis was applied to an SRTM-DEM and a hyperspectral image of the mountainous area of Calabria, Italy. The geometric correction was performed with the VITO-PAF. It would be sensible to apply the methodology to other case studies as well to gain more insights into the robustness of the method and the degree of error propagation in different circumstances.

From the results of the Monte Carlo analysis, we have calculated the standard deviations associated with the geometric corrections in the x and y coordinates. We have also calculated exceedance probability maps, which show the relative impact of DEM uncertainty on positional error, by considering the probability that the distortion in the x or y direction is greater than the pixel size. From the results, we have concluded that DEM uncertainty has an important effect on the geometric correction, as extended areas fail to reach the subpixel accuracies. The positional error is small in the flat terrain and in areas near the control points (small DEM uncertainty), and it is large in the rugged terrain and in areas far from the control points (large DEM uncertainty). The error increases with larger off-nadir viewing angles in the across-track direction, where the geometric correction algorithm is more sensitive to the elevation differences.

Even though it is well known that the positional error of the airborne imagery is larger in the rugged terrain and at a large off-nadir viewing angle, the generic Monte Carlo uncertainty propagation method proposed here quantifies the positional error pixel by pixel and thereby yields valuable information about the error magnitude and spatial distribution. This information is stored in the standard deviation and exceedance probability maps. These maps are an important contribution to the construction of so-called quality layers, which provide spatially explicit information about the accuracy associated with airborne imagery. This is an important development because end users require detailed information about the quality of their acquired products.

Acknowledgment

The authors would like to thank the Belgian Science Policy Office (BELSPO) for funding the LIDAR data in the framework of the BELSPO STEREO II project RAGALIRS (SR/67/61a and SR/67/61b) and the anonymous reviewers for their helpful comments. The AHS data were acquired in the framework of the European Facilities for Airborne Research Transnational Access Calabria project.

References

[1] R. J. Aspinall, W. A. Marcus, and J. W. Boardman, "Considerations in collecting, processing, and analysing high spatial resolution hyperspectral data for environmental investigations," *J. Geogr. Syst.*, vol. 4, no. 1, pp. 15–29, 2002.

[2] J. Biesemans, S. Sterckx, E. Knaeps, K. Vreys, S. Adriaensen, J. Hooyberghs, K. Meuleman, P. Kempeneers, B. Deronde, J. Everaerts, D. Schläpfer, and J. Nieke, "Image processing workflows for airborne remote sensing," in *Proc. 5th EARSeL Workshop Imaging Spectroscopy*, Bruges, Belgium, 2007.

[3] A. Hueni, J. Biesemans, K. Meuleman, F. Dell'Endice, D. Schläpfer, D. Odermatt, M. Kneubeuhler, S. Adriaensen, S. Kempenaers, J. Nieke, and K. I. Itten, "Structure, components, and interfaces of the airborne prism experiment (APEX) processing and archiving facility," *IEEE Trans. Geosci. Remote Sens.*, vol. 47, no. 1, pp. 29–43, Jan. 2009.

[4] M. Breuer and J. Albertz, "Geometric correction of airborne whiskbroom scanner imagery using hybrid auxiliary data," *Int. Arch. Photogramm. Remote Sens.*, vol. XXXIII, pp. 93–100, 2000.

[5] D. Schläpfer, J. Nieke, F. Dell'Endice, A. Hueni, J. Biesemans, K. Meuleman, and K. I. Itten, "Optimized workflow for APEX level 2/3 processing," in *Proc. 5th EARSeL Workshop Imaging Spectroscopy*, Bruges, Belgium, 2007.

[6] D. Schläpfer and R. Richter, "Geo-atmospheric processing of airborne imaging spectrometry data. Part 1: parametric orthorectification," *Int. J. Remote Sens.*, vol. 23, no. 13, pp. 2609–2630, Jul. 2002.

[7] K. M. Brown, G. M. Foody, and P. M. Atkinson, "Modelling geometric and misregistration error in airborne sensor data to enhance change detection," *Int. J. Remote Sens.*, vol. 28, no. 12, pp. 2857–2879, Jan. 2007.

[8] G. B. M. Heuvelink, *Error Propagation in Environmental Modelling With GIS*. London, U.K.: Taylor & Francis, 1998.

[9] D. Karssenberg and K. De Jong, "Dynamic environmental modelling in GIS: 2. Modelling error propagation," *Int. J. Geogr. Inf. Sci.*, vol. 19, no. 6, pp. 623–637, Jul. 2005.

[10] J. Oksanen and T. Sarjakoski, "Error propagation of DEM-based surface derivatives," *Comput. Geosci.*, vol. 31, no. 8, pp. 1015–1027, Oct. 2005.
[11] J. D. Brown and G. B. M. Heuvelink, "The data uncertainty engine (DUE): A software tool for assessing and simulating uncertain environmental variables," *Comput. Geosci.*, vol. 33, no. 2, pp. 172–190, Feb. 2007.
[12] G. B. M. Heuvelink, J. D. Brown, and E. E. Van Loon, "A probabilistic framework for representing and simulating uncertain environmental variables," *Int. J. Geogr. Inf. Sci.*, vol. 21, no. 5, pp. 497–513, Jan. 2007.
[13] P. Fisher, "Improved modeling of elevation error with geostatistics," *Geoinformatica*, vol. 2, no. 3, pp. 215–233, Oct. 1998.
[14] P. C. Kyriakidis, A. M. Shortridge, and M. F. Goodchild, "Geostatistics for conflation and accuracy assessment of digital elevation models," *Int. J. Geogr. Inf. Sci.*, vol. 13, no. 7, pp. 677–707, Oct. 1999.
[15] B. H. Carlisle, "Modelling the spatial distribution of DEM error," *Trans. GIS*, vol. 9, no. 4, pp. 521–540, Oct. 2005.
[16] P. F. Fisher and N. J. Tate, "Causes and consequences of error in digital elevation models," *Prog. Phys. Geogr.*, vol. 30, no. 4, pp. 467–489, 2006.
[17] H. I. Reuter, T. Hengl, P. Gessler, and P. Soille, "Preparation of DEMs for geomorphometric analysis," in *Geomorphometry: Concepts, Software, Applications*. Amsterdam, The Netherlands: Elsevier, 2009, pp. 87–120.
[18] K. W. Holmes, O. A. Chadwick, and P. C. Kyriakidis, "Error in a USGS 30-meter digital elevation model and its impact on terrain modeling," *J. Hydrol.*, vol. 233, no. 1–4, pp. 154–173, Jun. 2000.
[19] L. D. Raaflaub and M. J. Collins, "The effect of error in gridded digital elevation models on the estimation of topographic parameters," *Environ. Model. Softw.*, vol. 21, no. 5, pp. 710–732, May 2006.
[20] C. V. Deutsch and A. G. Journel, *GSLIB: Geostatistical Software Library and User's Guide*, 2nd ed. Oxford, U.K.: Oxford Univ. Press, 1998.
[21] J. M. Hammersley and D. C. Handscomb, *Monte Carlo Methods*. London, U.K.: Chapman & Hall, 1964.
[22] C. P. Robert and G. Casella, *Monte Carlo Statistical Methods*, 2nd ed. New York: Springer-Verlag, 2004.
[23] K. P. Van Niel, S. W. Laffan, and B. G. Lees, "Effect of error in the DEM on environmental variables for predictive vegetation modelling," *J. Vegetation Sci.*, vol. 15, no. 6, pp. 747–756, Dec. 2004.
[24] F. Hebeler and R. S. Purves, "The influence of elevation uncertainty on derivation of topographic indices," *Geomorphology*, vol. 111, no. 1/2, pp. 4–16, Oct. 2009.
[25] A. J. A. M. Temme, G. B. M. Heuvelink, J. M. Schoorl, and L. Claessens, "Geostatistical simulation and error propagation in geomorphometry," in *Geomorphometry: Concepts, Software, Applications*. Amsterdam, The Netherlands: Elsevier, 2009.
[26] P. Goovaerts, *Geostatistics for Natural Resources Evaluation*. New York: Oxford Univ. Press, 1997.
[27] N. A. C. Cressie, *Statistics for Spatial Data*, Revised ed. New York: Wiley, 1993.
[28] B. P. Marchant and R. M. Lark, "Optimized sample schemes for geostatistical surveys," *Math. Geol.*, vol. 39, no. 1, pp. 113–134, 2007.
[29] R. Webster and M. A. Oliver, *Geostatistics for Environmental Scientists*, 2nd ed. Chichester, U.K.: Wiley, 2007.
[30] P. A. W. Lewis and E. J. Orav, *Simulation Methodology for Statisticians, Operations Analysts, and Engineers*. Pacific Grove, CA: Wadsworth, 1989.
[31] A. Fernández-Renau, J. A. Gómez, and E. de Miguel, "The INTA AHS system," in *Proc. SPIE Sens., Syst., Next-Generation Satell. IX*, Bruges, Belgium, 2005, pp. 471–478.
[32] B. Rabus, M. Eineder, A. Roth, and R. Bamler, "The Shuttle Radar Topography Mission—A new class of digital elevation models acquired by spaceborne radar," *ISPRS J. Photogramm. Remote Sens.*, vol. 57, no. 4, pp. 241–262, Feb. 2003.
[33] A. Jarvis, H. I. Reuter, A. Nelson, and E. Guevara, "Hole-filled seamless SRTM data V4," International Centre for Tropical Agriculture (CIAT), 2008. [Online]. Available: http://srtm.csi.cgiar.org
[34] W. S. Walker, J. M. Kellndorfer, and L. E. Pierce, "Quality assessment of SRTM C- and X-band interferometric data: Implications for the retrieval of vegetation canopy height," *Remote Sens. Environ.*, vol. 106, no. 4, pp. 428–448, Feb. 2007.
[35] K. J. Bhang, F. W. Schwartz, and A. Braun, "Verification of the vertical error in C-band SRTM DEM using ICESat and Landsat-7, Otter Tail County, MN," *IEEE Trans. Geosci. Remote Sens.*, vol. 45, no. 1, pp. 36–44, Jan. 2007.
[36] M. A. King, "The GPS contribution to the error budget of surface elevations derived from airborne LIDAR," *IEEE Trans. Geosci. Remote Sens.*, vol. 47, no. 3, pp. 874–883, Mar. 2009.
[37] E. Honkavaara, "Calibration in direct georeferencing: Theoretical considerations and practical results," *Photogramm. Eng. Remote Sens.*, vol. 70, pp. 1207–1208, 2004.
[38] T. Moeller and B. Trumbore, "Fast, minimum storage ray-triangle intersection," *J. Graph. Tools*, vol. 2, no. 1, pp. 21–28, 1997.
[39] E. J. Pebesma and C. G. Wesseling, "Gstat: A program for geostatistical modelling, prediction and simulation," *Comput. Geosci.*, vol. 24, no. 1, pp. 17–31, Jan. 1998.
[40] E. J. Pebesma, "Multivariable geostatistics in S: The gstat package," *Comput. Geosci.*, vol. 30, no. 7, pp. 683–691, Aug. 2004.
[41] P. J. Diggle and P. J. Ribeiro, *Model-Based Geostatistics*. New York: Springer-Verlag, 2007.
[42] R. Ludwig and P. Schneider, "Validation of digital elevation models from SRTM X-SAR for applications in hydrologic modeling," *ISPRS J. Photogramm. Remote Sens.*, vol. 60, no. 5, pp. 339–358, Aug. 2006.
[43] I. Foster and C. Kesselman, *The Grid 2. Blueprint for a New Computing Infrastructure*. Amsterdam, The Netherlands: Elsevier, 2003.
[44] E. J. Pebesma and G. B. M. Heuvelink, "Latin hypercube sampling of Gaussian random fields," *Technometrics*, vol. 41, no. 4, pp. 303–312, Nov. 1999.
[45] R. Richter and D. Schläpfer, "Geo-atmospheric processing of airborne imaging spectrometry data. Part 2: atmospheric/topographic correction," *Int. J. Remote Sens.*, vol. 23, no. 13, pp. 2631–2649, Jul. 2002.
[46] R. Richter, "Correction of atmospheric and topographic effects for high spatial resolution satellite imagery," *Int. J. Remote Sens.*, vol. 18, no. 5, pp. 1099–1111, Mar. 1997.

Johan Beekhuizen received the M.Sc. degree (with distinction) in geoinformation science from Wageningen University, Wageningen, The Netherlands, in 2008, where his thesis focused on determining the optimal location of mobile measurement devices in case of contaminant dispersion using geostatistics and optimization techniques.

He did his internship at the University of California, Santa Barbara, in 2008, where he worked on a computational framework that is used to improve land cover classification of satellite imagery. After his studies, he became a Researcher at the European Facilities for Airborne Research, developing an uncertainty propagation concept for airborne hyperspectral imagery. He is currently with the Institute for Risk Assessment Sciences (IRAS), Utrecht University.

Gerard B. M. Heuvelink received the M.Sc. degree in applied mathematics from Twente Technical University, Enschede, The Netherlands, in 1987 and the Ph.D. degree in environmental sciences from Utrecht University, Utrecht, The Netherlands, in 1993.

From 1991 to 2003, he worked as an Assistant Professor in geostatistics and stochastic simulation with the University of Amsterdam, Amsterdam, The Netherlands. Since 2003, he has been a Senior Research Scientist in geostatistics with Alterra and an Associate Professor in pedometrics with the Department of Environmental Sciences, Wageningen University, Wageningen, The Netherlands. He has written over 140 scientific publications on geostatistics, spatial uncertainty analysis, and pedometrics, with about 50 of which appeared in peer-reviewed international journals. He has been involved in many research projects that deal with spatial uncertainty in environmental modeling and spatial analysis, and he is recognized worldwide as a leading scientist in pedometrics and spatial uncertainty analysis, mainly through his publications (notably his book *Error Propagation in Environmental Modelling with GIS*) and active involvement as a program committee member in various GIS and accuracy-related conference series. He is an Associate Editor of the *European Journal of Soil Science* and an Editorial Board Member of *Geoderma*, *Transactions in GIS*, *Environmental and Ecological Statistics*, and *International Journal of Applied Earth Observation and Geoinformation*.

Dr. Heuvelink chaired the Pedometrics Commission of the International Union of Soil Sciences from 2003 to 2006, and he was the President of the Netherlands Soil Science Society from 2004 to 2007. He is a member of the *Board for Sciences of the Earth and Space* of the *Flanders Fund for Scientific Research*.

Jan Biesemans received the M.Sc. and Ph.D. degrees in agricultural and applied biological sciences (soil physics and hydrology) from Ghent University, Ghent, Belgium, in 1995 and 2000, respectively.

After five years of academic research and teaching activities, he worked for about two years as a C++ Software Development Engineer in the prepress industry. After this period, he worked for two years as an Independent Consultant for private, governmental, and intergovernmental organizations, focused on the generation of custom-made software solutions for specific data analysis problems in the field of spatial epidemiology and modeling of environmental processes. In June 2004, he then became a Project Coordinator with the Flemish Institute for Technological Research (VITO), Mol, Belgium, where he currently coordinates in software development activities with respect to Unmanned Aerial Vehicle ground segments and specific airborne imaging projects.

Ils Reusen received the M.Sc. degree in physics (astronomy) and the Ph.D. degree in physics (nuclear astrophysics and spectroscopy) from the Katholieke Universiteit Leuven (K.U.Leuven), Leuven, Belgium, in 1993 and 1999, respectively.

After her Ph.D. degree, she had a six-month Postdoc position in image processing with the Electrical Engineering Department, K.U.Leuven. After that, she joined the Research Unit Remote Sensing and Earth Observation Processes, Flemish Institute for Technological Research (VITO), Mol, Belgium. She has been active in airborne hyperspectral remote sensing since 2000. She was involved in the development of the imaging spectrometer "Airborne Prism Experiment (APEX)" for the European Space Agency. She coordinated the development of the HyperTeach training course material and organized international HyperTeach training courses in 2005, 2006, and 2007 in Belgium, Turkey, Indonesia, and South Africa. She was coordinating the FP6 HYRESSA project from 2006 to 2008. She is currently coordinating the FP7 EUFAR HYQUAPRO project on the development of quality layers for airborne hyperspectral data. Her research includes the radiometric calibration of the future PROBA-V Earth Observation sensor using ground-based hyperspectral reflectance measurements and APEX underflights.

Dr. Reusen is a member of the scientific committees of EARSeL SIG Imaging Spectroscopy, WESSEX Forest Fires, and Whispers. She is a member of the ISPRS Technical Commission I Working Group 1 "Standardization of Airborne Platform Interface." In 2007, she chaired the international 5th EARSeL SIG Imaging Spectroscopy workshop.